DARU Journal of Pharmaceutical Sciences (2020) 28:171–180
https://doi.org/10.1007/s40199-020-00328-x

RESEARCH ARTICLE

Amphiphilic hyperbranched polyester coated rod mesoporous silica nanoparticles for pH-responsive doxorubicin delivery

Reza Bafkary[1] · Shirin Ahmadi[1] · Faeze Fayazi[1] · Mehdi Karimi[1] · Yousef Fatahi[1] · Seyed Mostafa Ebrahimi[1] · Fatemeh Atyabi[1] · Rassoul Dinarvand[1]

Received: 1 May 2019 / Accepted: 16 January 2020 / Published online: 31 January 2020

Abstract

Rod-like mesoporous silica nanoparticles with pH-responsive amphiphilic hyperbranched polyester shells were prepared for doxorubicin (DOX) delivery. First, rod-shaped mesoporous silica nanoparticles (MSNs) were obtained, then hydrophobic hyperbranched polyester Boltorn H40 (H40) was grafted on their surface. The H40 coated MSNs were next treated with amine-functionalized polyethylene glycol (PEG) to achieve the hydrophilic and pH-responsive material denoted as PEG-H40-MSNs. The experimental results showed that PEG-H40-MSNs were successfully synthesized. BET analysis showed that rod MSNs exhibits a type IV standard isotherm. TEM revealed that the thin gray polymer layer was formed around the SBA-15 particle with a diameter of around 150 nm. DOX was effectively loaded, which can be released according to the ambient pH inside the cell as follow: at pH 7.4, only 9.7% of the DOX was released after 48 h; as the pH decreased to 5.5, the cumulative release reached to 49% at the same time. PEG-H40-MSNs showed less than 1.6% of hemolytic activity and a slight effect on the liver and kidney of treated mice were observed at a high disposal dosage implying negligible toxicities were caused by PEG-H40-MSNs in both in vitro hemolysis analysis and in vivo biochemical in mice. However, the in vitro cytotoxicity evaluation of the DOX-PEG-H40-MSNs showed that the cell cytotoxicity of both pure DOX and DOX-loaded PEG-H40-MSNs generally enhanced by increasing the concentration of DOX.

Keywords Mesoporous silica nanoparticles · Hyperbranched polyester · pH-responsive drug delivery

Introduction

In recent years, the number of published studies that focused on investigating stimuli-responsive nanocarriers as a promising tool to improve the effectiveness of target-drug delivering in medical therapy has been dramatically increased [1, 2]. In this respect, Smart nanocarriers could provide the possibility of safe drug delivery to diseased cells without damaging healthy cells and reducing associated side effects [3].

Among the so far developed nanocarriers, organic-inorganic hybrid nanocarriers based on utilizing polymeric materials as organic part and mesoporous silica materials as inorganic part have gained much interest. A variety of inorganic materials have been used to fabricate polymeric based nanocarriers. Among them, mesoporous silica nanoparticles (MSNs) type SBA-15 have a special status in the area of efficient drug delivery platform due to their unique features such as highly robust and stable structure, high drug loading capacity, great biocompatibility, high specific surface area and high and tunable pore diameters [4].

Many types of research have focused on the effects of shape, particle size, type of surface modification on the drug delivery performance and cellular uptake of different MSNs in recent years [5–8]. For instance, Chun Xu and Yu have individually proved that rod-shaped MSNs enhances the cellular uptake compared with spherical ones [9, 10].

Fortunately, the presence of abundant –OH groups on the surface of MSNs and availability of various silanol functionalities allow anchor various types of materials such as PEG, chitosan, Poly (N-isopropyl acrylamide) and aliphatic hyperbranched polymeric materials onto their surface to subsequently convert them to a smart nanocarrier [11, 12].

One of the most well-known aliphatic hyperbranched polymeric materials with the acceptable ability for drug loading is

✉ Rassoul Dinarvand
dinarvand@tums.ac.ir

[1] Tehran University of Medical Sciences, Tehran, Islamic Republic of Iran

2,2-bis(methylol)propionic acid branching unite or Boltorn H40 (H40). H40 is known for its simple synthesis route, amphiphilic core-shell structure, low toxicity, degradability into lower molecular weight, compatibility in biological environments, commercial availability, and possessing a large number of terminal functionalities which provide better interactions with drug molecules [13]. Despite all these advantages, H40 may not be used directly due to its hydrophobic structure and easy recognition and removal by macrophages. Therefore, it needs to be modified with biocompatible and hydrophilic polymers such as PEG, which also restricts the amount of uptake by macrophages. Hence, the permeability of nanocarriers and the efficiency of drug delivering will be enhanced [14].

Modification of H40 with tertiary amine PEGs enables it to show both hydrophilicity and pH responsiveness behaviors and works from the physiological environment (pH 7.4) to cancer and tumors cells (pH 5.5). The prominent feature of this hybrid is that H40 swells at low pH and shrinks at higher pH one, therefore, allows opening and closing the pores of MSNs and the diffusion of drug molecules in and out of the pores respectively. Also, due to the fact that the cell surface has a negative charge, the cellular uptake of nanoparticles enhances with the surface modification by a positively charged polymer [15].

In this study, a novel hybrid nanocarrier based on rod-shaped mesoporous silica and the pH-responsive polymeric shell composed of PEG and also tertiary amine decorated on H40 through grafting diethylaminopropylamine (DEAPA) and m-PEG to hydroxyl end groups of polyester for DOX delivery is reported. The synthesized hybrid nanoparticles displayed essential features that are required for drug delivery, such as lower toxicity, acceptable biocompatibility, and the ability to control DOX release in different pHs (Fig. 1).

Materials and methods

Materials

Tetraethyl orthosilicate (TEOS), N,N′-Dicyclohexylcarbodiimide (DCC), 4-(Dimethylamino) pyridine (DMAP), thionyl chloride, succinic anhydride, toluene, tetrahydrofuran (THF), Boltorn-H 40, N-Methyl-2-pyrrolidone (NMP), acetone, dioxane, pyridine, DEAPA, carbonyldiimidazole (CDI), 3-aminopropyltriethoxysilane (APTES) and Pluronic P123 ($EO_{20}PO_{70}EO_{20}$, Mac = ca. 5800) were purchased from Sigma Aldrich. O-Methyl-O′-succinylpolyethylene glycol 1000 (mPEG-COOH 1000) was purchased from Nanocs Inc. Doxorubicin, in the form of hydrochloride salts, was purchased from Korea United Pharm. INC (Chungnam, Korea). Deionized water used for all experiments was purified with a Milli-Q water system. All the chemicals were of analytical grade and used without purification except for THF, which were further purified. Human red blood cells (HRBCs) stabilized with EDTA were prepared from Iran Blood Transfusion Institute. The bouncing male Balb/c mice (bodyweight about 20 g and 5–6 weeks) were prepared from Pasteur Institute, Tehran, Iran.

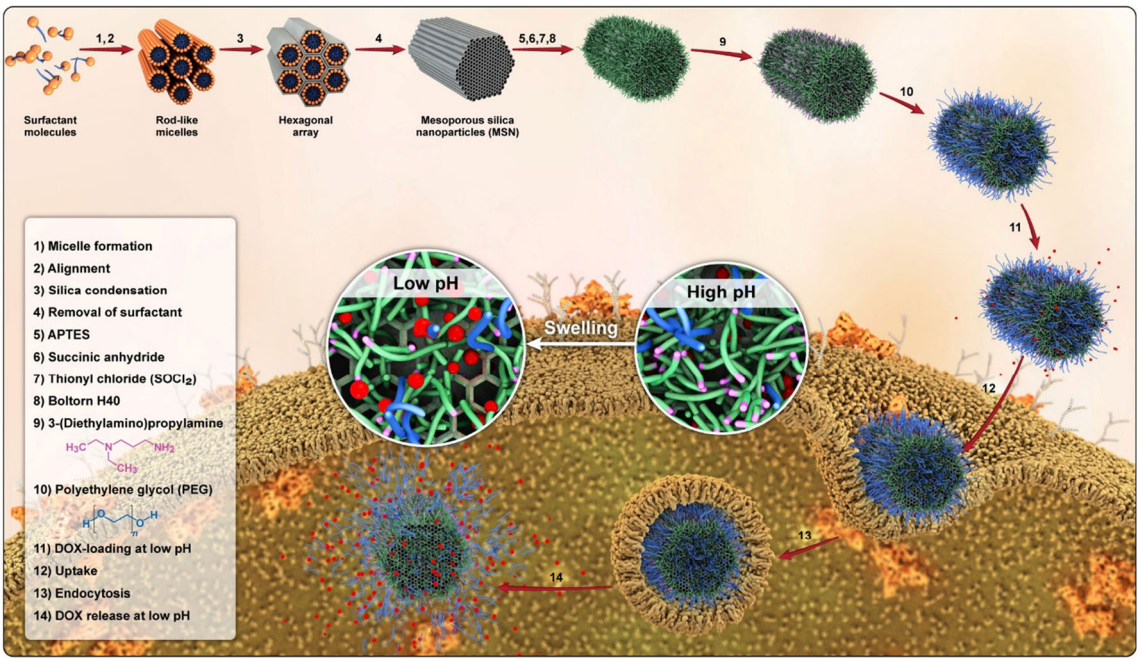

Fig. 1 Schematic pattern for preparation, cellular uptake and DOX release of PEG-H40-MSNs

Instrumentation

Fourier transform infrared (FTIR) spectroscopy (Bruker, Germany) was used by the KBr disk method over the range 400–4000 cm^{-1} with the resolution of 2 cm^{-1}. Transmission electron microscope (TEM) operating at an accelerating voltage of 80 kV by Zeiss-EM10C was used and samples were prepared by placing ultrasonicated drops of PEG-H40-MSNs suspension onto Formvar carbon-coated grid Cu Mesh 300. The grid was wholly dried and used for TEM analysis. Thermogravimetric analysis Q50 V6.3 Build 189 was conducted at a rate of 10 °C/min under nitrogen blanket over the temperature range from 25 to 600 °C. Ultraviolet-visible spectroscopy (UV-Vis) carry 100 Bio spectrophotometer was used. Dynamic light scattering (DLS) and Zeta measurements were used with Malvern Zetasizer Nano-ZS (Malvern Instruments, Malvern, UK) at 25 °C. X-ray diffraction (XRD) pattern was conducted with Bruker D8FOCUS X-ray diffractometer.

N_2 adsorption-desorption isotherms were performed by BELSORP-miniII instrument at liquid nitrogen temperature.

Synthesis of amine-functionalized SBA-15 (MSN-NH_2)

SBA-15 was synthesized based on the Karimi and et al. procedure [16]. Briefly, Pluronic P123 (11.7 g) and HCl (73.3 g) were poured in deionized water (303.4 mL) and stirred for 3 h at 55 °C. Next, TEOS (25 g) was added to the above solution and the reaction continued for 24 at 55 °C. Afterward, the reaction vessel was kept in a 100 °C oven for 24 h and, then, resultant product was centrifuged and dried at room temperature. To synthesis amine-modified MSNs, APTES (1 mL) was added to SBA-15 (1 g) suspended in toluene (80 mL) and the mixture was refluxed for 24 h. Finally, the resultant product was washed several times with ethanol/HCl solution for removing the surfactant. The final amine-functionalized SBA-15 was denoted as MSN-NH_2.

The synthesis of acyl chloride functionalized MSNs

100 mg of prepared MSN-NH_2 was suspended into 5 mL acetone under the stirring condition at room temperature for 4 h. Then, 3.5 mL acetone solution containing 1.5 M succinic anhydride was dropwisely added and stirred at room temperature for another 24 h resulting in carboxylic acid functionalized SBA-15 powder (MSN-COOH) which was then filtered and washed with an excess amount of deionized water and ethanol to remove the remaining solvents and dried overnight at ambient temperature. Dried MSN-COOH was reacted with excess neat $SOCl_2$ (5 mL) at 70 °C for 24 h. The residual $SOCl_2$ was removed under vacuum, with yield of around 88%. Final Acyl chloride functionalized MSNs were denoted as MSN-COCl.

Synthesis of hyperbranched MSN-15 (H40-MSN)

To a 100 mg H40 dissolved in 10 mL dioxane was added 3 drops of pyridine as acid-neutralizing agent followed by adding 50 mg of MSN-COCl. After that, the reaction vessel was kept in an ultrasound bath for 1.5 h. Next, the temperature of the reaction mixture was elevated to 70 °C and kept constant for 24 h at this temperature. The resulting precipitate was collected with a centrifuge at room temperature and washed several times with deionized water and, then, dried at 40 °C for 24 h in a vacuum oven resulting in a 79% yield. The final product was denoted as H40-MSN.

Synthesis of DEAPA–carbonylimidazole (DEPA-CDI)

DEPA-CDI was synthesized based on the Reul and et al. procedure [13]. Dry THF (15 mL) under argon atmosphere was inserted into a round-bottomed flask equipped with a gas inlet and a septum cap. Then, CDI (2.71 g, 16.7 mmol) was added to THF. For obtaining an equivalent molar ratio of CDI:DEAPA, DEAPA (2.18 g, and 16.7 mmol) was injected at 60 °C, and the reaction was continued for 20 h at 25 °C. Finally, the solvent was evaporated to obtain oily and slight yellow products. The resultant was denoted as DEPA-CDI.

Synthesis of DEAPA decorated H40-MSN

To a dispersion of H40-MSN (75 mg) in NMP (1 mL), a solution of DEPA-CDI (0.115 g, 0.39 mmol) in NMP (0.7 mL) was dropwisely added and, then, 0.072 g of DMPU was poured to the vessel and the reaction continued for 5 days at 80 °C. The resulted product denoted as aminated H40-MSN was centrifuged five times and dried in a vacuum oven.

Synthesis of PEG decorated H40-MSNs

A mixture of H40-MSNs (50 mg), mPEG-COOH (0.5 g), and DMAP (1 mmol) in anhydrous DMF (40 mL) was prepared and sonicated in a probe-type sonicator for 10 min (5 s on/2 s off). Then, anhydrous DMF (10 mL) containing DCC (0.01 mol) was dropwisely added and the reaction was continued for 12 h at 30 °C. In the end, the resulting precipitate was collected by a centrifuge at room temperature and washed with deionized water and ethanol several times and, finally, freeze-dried. The obtained nanocarrier was denoted as PEG-H40-MSNs.

DOX loading and release

In order to load DOX into PEG-H40-MSNs, 10 mg of nanoparticle and 10 mg of DOX hydrochloride were treated with 2 mol of triethylamine dissolved in 3 mL of DMF and 7 mL deionized water at 4 °C with pH of 3.0 with stirring for 24 h in

the dark place. Then, pH was adjusted to 8.0 followed by stirring the solution for further 2 h. Subsequently, DOX-loaded PEG-H40-MSNs separated by centrifuge was washed twice by a NaOH solution with a pH of 8.0. The drug loading content was determined by the following equation:

To measure the percentage of drug release, 1 mg DOX-loaded PEG-H40-MSNs were suspended in 2 mL fresh phosphate buffer solution followed by stirring at 120 rpm at 37 °C. Then, at a predetermined interval, an aliquot of the supernatant was taken. The Encapsulation efficiency was determined by the following equation:

To simulate the related biological conditions, pH values were adjusted to 5.5, 6.8, and 7.4. UV-Vis measurements at a wavelength of 480 nm (three times for each sample) were recorded to calculate the amount of loaded DOX into the nanocarriers. By using the provided UV-Vis data and the equations of (1) and (2), both the drug loading content and the Encapsulation efficiency were estimated.

$$\textit{Drug loading content}\ (\%) = \frac{\textit{Weight of the drug in particles}}{\textit{Weight of the particles}} \times 100 \quad (1)$$

$$\textit{Etrapment efficiency}\ (\%) = \frac{\textit{Weight of the drug in particles}}{\textit{Weight of the feeding drug}} \times 100 \quad (2)$$

In vitro cytotoxicity

The MCF-7 cells were used to investigate the in vitro cytotoxicity. The cells which seeded in 96-well cell culture plate (density of 1×10^4 cells per well) were cultured under 5% CO_2 at 37 °C for 24 h. After removing media, the cells were exposed to a fresh medium with various concentrations of free drug, pure nanocarrier, and drug-loaded nanocarrier or various pH values, containing the same concentration of DOX followed by further incubation for 48 h. Then, 20 μL of 5.0 mg/mL MTT solution was added into each well and they were incubated for another 4 h. Then, the supernatants were eliminated and, then, 150 μL DMSO was poured into each well. Finally, the absorbance of the obtained solutions was recorded at 570 nm, and data were reported as means ± SD.

Hemolysis assay

In vitro cellular uptake measurements were conducted according to the method described in our previous work [11]. The HRBCs were collected by eliminating the serum from the blood using a centrifuge and washing it with sterile isotonic PBS solution five times. Then, following solutions were obtained by mixing 0.3 mL of a diluted mixture of the cells and PBS solution with a) 1.2 mL deionized water as a positive control; b) 1.2 mL PBS as negative control, and c) 1.2 mL suspension of PEG-H40-MSNs with the concentrations of 50, 100, 200, and 400 $\mu g mL^{-1}$. After moderately shaking, suspensions were standing for 2 h at ambient temperature followed by centrifuging and recording absorbance spectra of the supernatants in the range of 500 to 600 nm. Finally, dividing the difference between the sample and the negative control absorbance by the difference between negative and positive control absorbance both recorded at 541 nm gave the hemolysis values of the samples.

In vivo toxicity studies

The healthy bouncing male Balb/c mice (body weight about 20 g and 5–6 weeks) were obtained from Pasteur Institute, Tehran, Iran. The study was approved by the Institutional Animal and Ethics Committee (Faculty of Pharmacy, Tehran University of Medical Sciences, Iran). According, 0.2 mL dispersion of PEG-H40-MSNS in physiological saline (10 $mg.kg^{-1}$) was injected into Balb/c mice ($n = 5$ per group) through the tail vein. Balb/c mice injected just by physiological saline was chosen as a control group.

Serum biochemical analysis

After 4 h and also 10 days after injection and before scarifying the mice, the blood samples were taken from an ophthalmic vein and, then, the serums were separated using a centrifuge at 3500 rpm for 10 min. In this step, most important kidney functions (blood urea nitrogen creatinine and (BUN)) and hepatic indexes (aspartate and alanine aminotransferase (ALT) aminotransferase (AST)) were characterized.

Results

XRD analysis

Figure 2 represents the XRD patterns of the rod-shaped mesoporous silica powder. Generally, mesoporous silica materials exhibit three diffractions, one intense diffraction around $2\theta = 1°$ reflected from (100) plane and two weak diffractions around $2\theta = 1.8°$ reflected from (110) and (200) planes. The existence of these three diffractions together in XRD patterns confirms the formation of long-range periodic order and two-dimensional hexagonal (p6mm) mesostructure. Since those above-mentioned diffractions were a presence in Fig. 2, it can be concluded that this rod mesoporous silica possesses the specific structure of SBA-15.

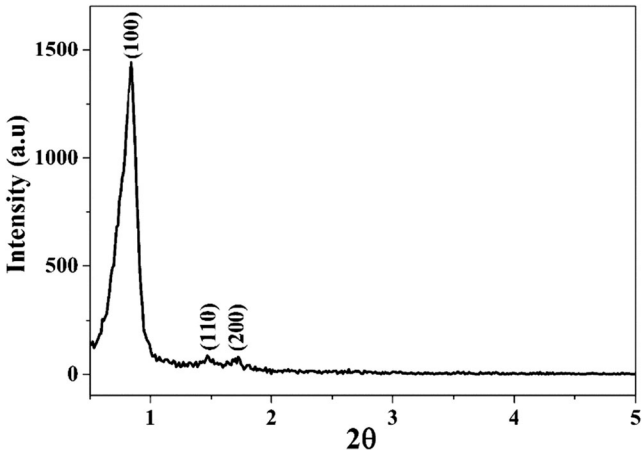

Fig. 2 XRD patterns of rod MSN

FTIR analysis

Figure 3 showed the main FTIR spectra of the synthesized materials. The FTIR spectrum of the aminated SBA-15 showed two weakly peaks at 1310 cm^{-1} and 1381 cm^{-1} attributed to the C − N group stretching bands (Fig. 3a). Two peaks at 1476 cm^{-1} and 1563 cm^{-1} were associated with the bending vibration of N − H groups [17]. A clear visible band at 1100 cm^{-1} corresponded to the Si − O − Si groups. After grafting Boltorn H40 on the surface of MSN, significant differences at several wavelengths appeared (Fig. 3b). A large absorption band at 3440 cm^{-1} was ascribed to the hydroxyl end groups on the hyperbranched Boltorn H40. The characteristic absorption bands of the carbonyl ester groups were shown at 1729 cm^{-1} [13]. The peaks around 1223 cm^{-1} and two weakly sharp peaks at 2955 cm^{-1} and 2884 cm^{-1} were suggested to be caused by the ether groups and the aliphatic −CH2− of Boltorn H40, respectively. In the FTIR spectra of the aminated H40-MSN, a new peak appeared at 1705 cm^{-1} was related to the carbamate bond (Fig. 3c) accompanied by decreasing the intensity of the broad band of hydroxyl groups around 3400 cm^{-1}. At the same time, the intensity of broad peaks at 3400 cm^{-1} significantly increased and the intensity of carbonyl ester groups of boltorn H40 at 1732 cm^{-1} decreased for PEG-H40-MSNs, which related to the presence the PEG (Fig. 3d).

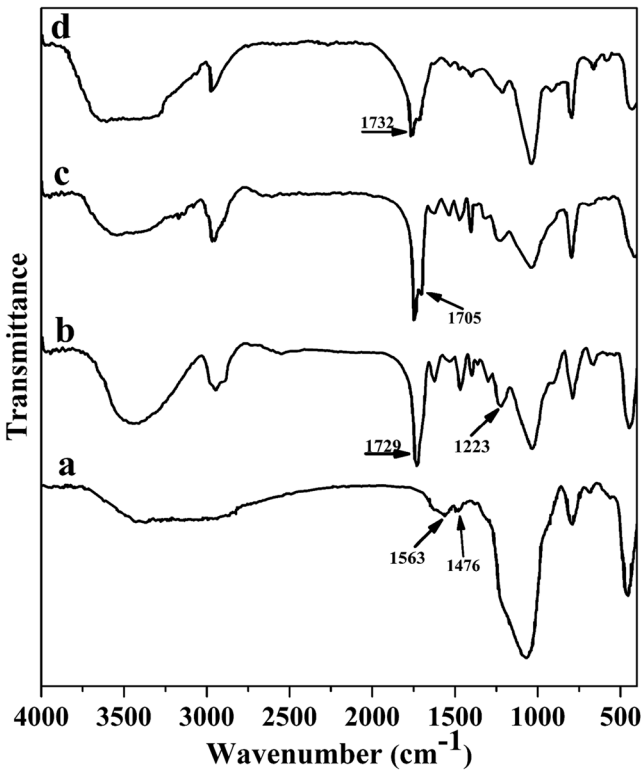

Fig. 3 FTIR spectra of a) MSN-NH2, b) H40-MSN c) aminated H40-MSN, and d) PEG-H40-MSNs

Nitrogen adsorption and desorption analysis

The mesoporous nature of the SBA-15 and PEG-H40-MSNs were investigated by N_2 adsorption and desorption measurements. Ordered mesoporous silica material, generally, exhibits a type IV standard IUPAC isotherm with an H1 type hysteresis loop and sharp capillary condensation steps at P/P_0 of 0.6–0.8. According to Fig. 4a and b, the isotherms of both samples showed characteristics of mesoporous materials. Moreover, an important conclusion is that the mesoporous nature of SBA-15 particles was well preserved after modification steps.

TEM analysis

Figure 5 provided the representative TEM images of SBA-15 and PEG-H40-MSNs. Figure 5a and b related to TEM images of free surfactant SBA-15 displayed straight and parallel channels within the particle, which further confirmed the results from XRD and N_2 adsorption-desorption analyses.

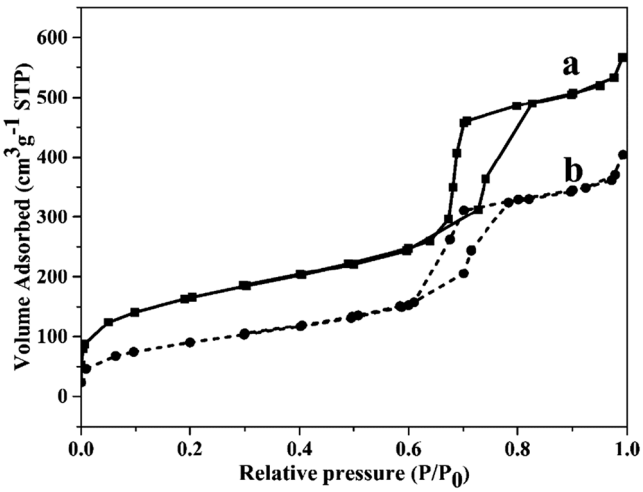

Fig. 4 Nitrogen adsorption-desorption isotherms result of (a) SBA-15 and (b) PEG-H40-MSNs

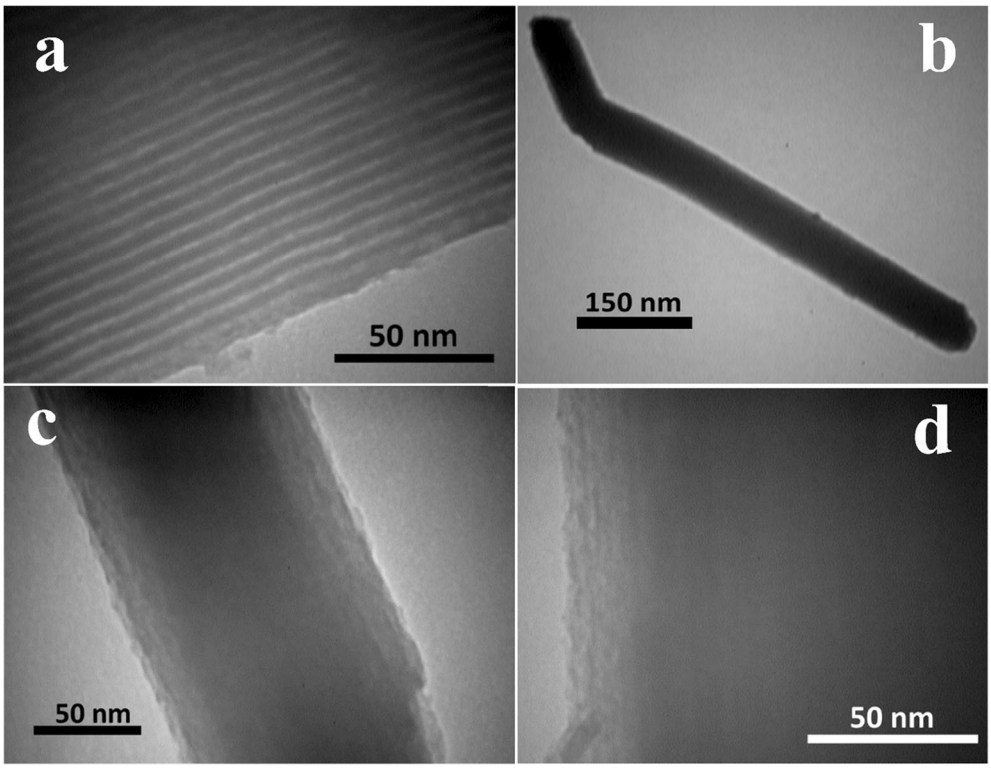

Fig. 5 TEM images of MSN (a) (magnification 160,000) and PEG-H40-MSNs (b) (magnification 160,000), (c) (magnification 160,000), (d) (magnification 160,000)

Thermogravimetric analysis

The thermogravimetric curves of MSN and PEG-H40-MSNs were also obtained to investigate the amount of the grafted organic part on the surface PEG-H40-MSNs sample (Fig. 6). The mass loss below 150 °C was assigned to the removal of physisorbed water molecules on the surface, which was about 5% for PEG-H40-MSNs. Moreover, the mass loss above 150 °C could be assigned to the decomposition of the polymeric shell, which was about 50% for PEG-H40-MSNs.

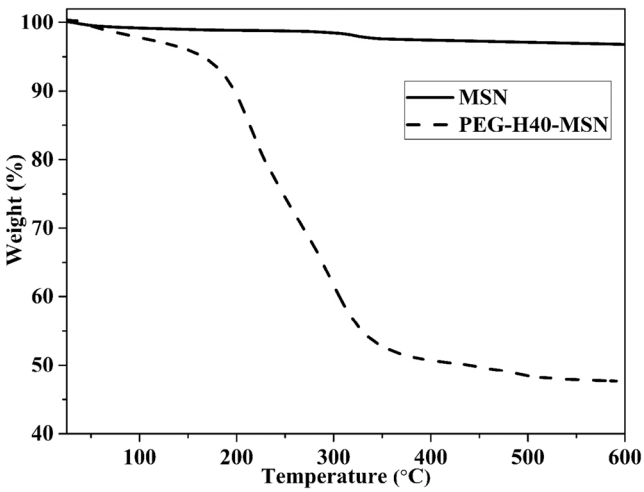

Fig. 6 TGA curves of MSN and PEG-H40-MSNs

DOX loading and releases

DOX was used as a model drug in this work. Based on the equation of 1 and 2, nanocarriers exhibited great drug loading capacity and Encapsulation efficiency, which were calculated to be 36.5 ± 3.9% and 57.4 ± 4.2%, respectively.

In vitro release behavior of DOX-loaded PEG-H40-MSNs was evaluated at 37 °C under pH values of 7.4 (blood circulation), 6.8 (tumor extracellular), and 5.5 (endosomes) for 48 h. From the obtained results pictured in Fig. 7, it can be observed that the rates of DOX release from the nanocarrier

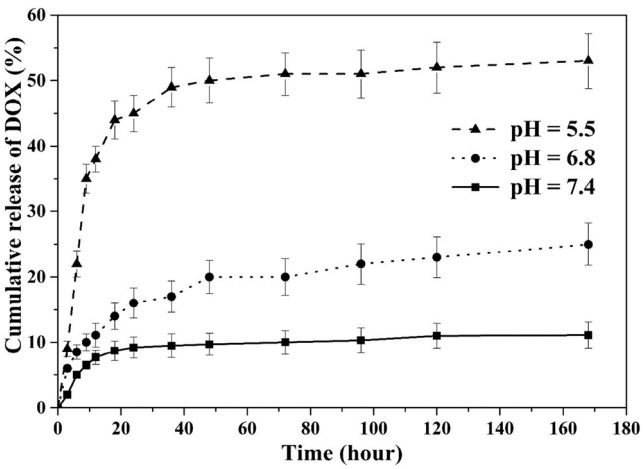

Fig. 7 Release profiles of DOX from PEG-H40-MSNs at different pH values

were different in various pH values, i.e., the released amount of DOX was only 9.7% and 20% at pH 7.4 and pH 6.8, respectively, in the first 48 h; while it reached to 49% at pH 5.5 at the same amount of time.

In vitro blood compatibility

Hemolysis assays were conducted to evaluate the blood compatibility of the nanocarrier at various concentrations. The depicted results in Fig. 8 showed negligible effects of PEG-H40-MSNs over a broad concentration range of 0–400 μgmL^{-1}. In addition, the obtained results from the absorbance of the supernatant at 541 nm (hemoglobin) to evaluate the hemolytic activity of the specimens showed less than 1.6% of hemolytic activity for the PEG-H40-MSNs at a high concentration. These results proved the great biocompatibility of the vectors with blood cells which make it suitable for intravenous injection.

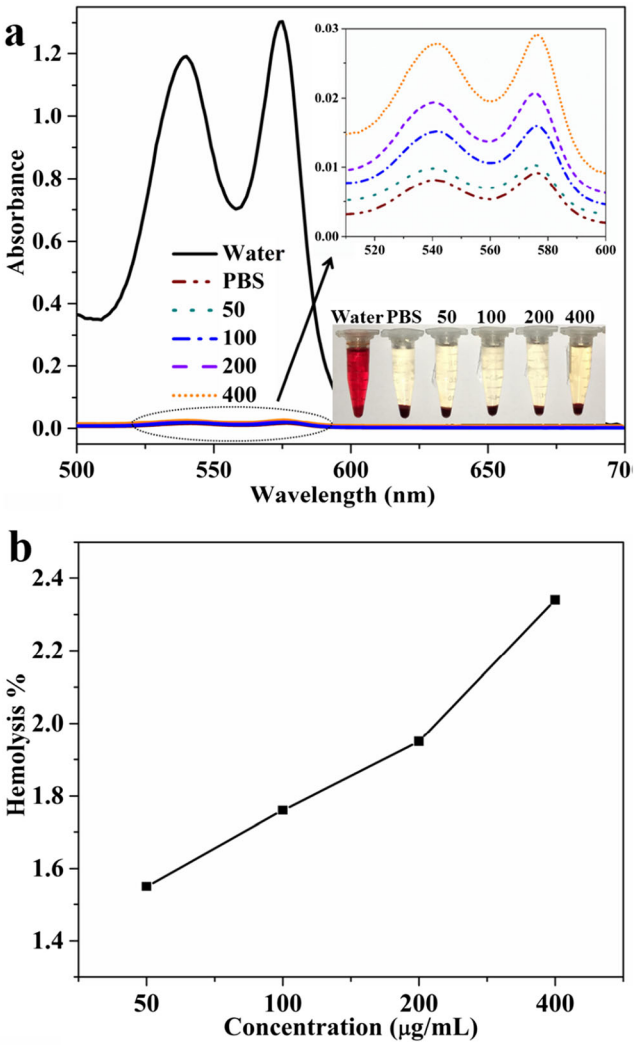

Fig. 8 (a) The UV-vis absorption spectra and visually observation (the bottom-right inset) to detect the presence of hemoglobin in the supernatant of PEG-H40-MSNs suspensions, b) hemolysis percentages measured of HRBCs by PEG-H40-MSNs at various concentrations

In vivo toxicity studies

The predefined values of PEG-H40-MSNs (dose = 10 mg.kg^{-1}) were injected into the tail vein of Balb/c mice intravenously. All of the treated mice had normal behavior during the experimental period and did not show any infection and impaired mobility. Moreover, no reduction in feeding was observed which was a sign of non-toxicity of PEG-H40-MSNs.

Ophthalmic veins were used for obtaining the blood samples before scarifying mice after 5 h and 10 days from the injection. The serum was separated by centrifuge and kidney functions (BUN and creatinine) and hepatic indexes (ALT and AST) were specified.

ALT and AST, two important liver health indicators of two groups of treated mice (5 h and 10 days after injection), which were very close and had a good match with the control group (Table 1). Also, kidney health functions (BUN and creatinine) had negligible diversity in contrast with the control mice (Table 1).

In vitro cytotoxicity of DOX-loaded PEG-H40-MSNs

The cell viability of free DOX and DOX-PEG-H40-MSNs nanoparticles on the MCF7 cell line were evaluated by MTT assay in vitro at pH 7.4 related to the normal physiological pH. According to Fig. 9, the cell cytotoxicity of both pure DOX and DOX-PEG-H40-MSNs generally enhanced by increasing concentration of DOX and free DOX represented more cytotoxicity than DOX-PEG-H40-MSNs at the same DOX dosage, except for samples with 2 and 5 μg/mL of DOX where no noteworthy changes were detected. These observations were probably due to the possibility that drug loading in PEG-H40-MSNs required to spend more time to enter into the nucleus of the cell than free pure DOX.

Table 1 Biochemistry assay of PEG-H40-MSNS nanoparticles on Balb/c mice serum 4 h and 10 days after treatment

Chemistry	Control	Treated mice [mouse $^{-1}$]	
	0	4 h	10 d
BUN (mM) [mg dL^{-1}]	40 ± 5	39 ± 6	38 ± 6
Creatinine [mg dL^{-1}]	0.7 ± 0.05	0.7 ± 0.02	0.6 ± 0.09
AST [U L^{-1}]	141 ± 14	137 ± 15	143 ± 16
ALT [U L^{-1}]	75 ± 9	75 ± 9	78 ± 10

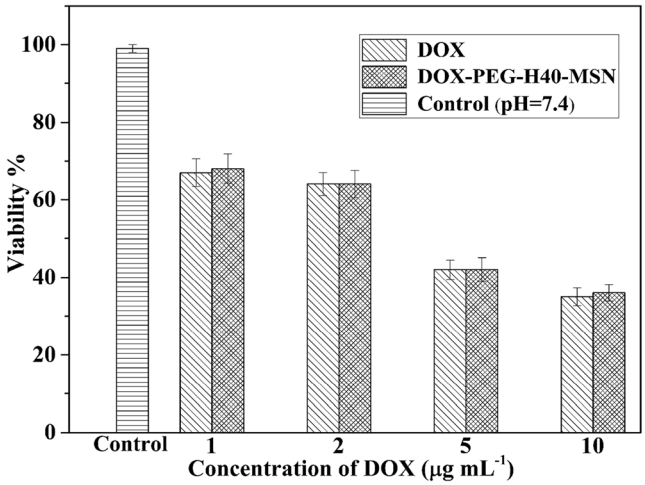

Fig. 9 pH-dependent cytotoxicity of DOX and DOX-PEG-H40-MSNs in different concentrations. Results were expressed as mean ± SD ($n = 5$)

Discussion

In order to prepare the pH-responsive and biocompatible nanocarrier for drug delivery, SBA-15 was firstly synthesized using Pluronic P123 as a structure-directing agent. Then, the outer surface of as-synthesized SBA-15 particles was aminated with APTES before removing pluronic p123 to keep the inner surface inside the channel intact for allowing effective drug loading subsequently. Afterward, pluronic P123 was eliminated to open the channels. In the next stage, the aminated surface of SBA-15 was activated by reacting it, first with succinic anhydride and, then, with thionyl chloride to obtain acyl chloride functionalized SBA-15. Boltorn H40 was grafted to this product to obtain hyperbranched polyester grafted SBA-15 and, then, it was modified by tertiary aminated and PEG 1000. For modifying hyperbranched polyester with a tertiary amine, activated DEAPA with carbonyldiimidazole was used and reacted with hydroxyl groups to form carbamate linkage. In the end, activated PEG-COOH via DCC and DMAP reacted with remained hydroxyl groups of hyperbranched polyester.

The lower volume of gas adsorption in BET analysis in PEG-H40-MSNs showed its effect on lower levels of hysteresis loop that means there was still sufficient space to load drugs inside the mesoporous channels [18]. S_{BET}, V_P, and d_P of SBA-15 were found to be 453 $m^2.g^{-1}$, 4.03 nm, and 0.7913 $cm^3\ g^{-1}$, respectively, which decreased to 682 $m^2\ g^{-1}$, 0.87 $cm^3\ g^{-1}$ and 2.6 nm, respectively, for PEG-H40-MSNs indicating there is still much free space inside the channels for DOX loading. However, reduction of average pore diameter (d_P), surface area (S_{BET}), and pore volume (V_P) due to grafting amphiphilic pH-responsive shell onto the surface of rod-shaped MSNs resulted in a lower level of adsorbed N_2 gas.

TEM images illustrated in Fig. 5c and d related to PEG-H40-MSNs showed the thin gray layer related to a polymer formed around the SBA-15 particle which blocked the channels to be observed. Furthermore, a rod-type shape with a diameter less than 150 nm was observed in these images and the size of particles did not show meaningful changes compared to the initial SBA-15.

Zeta potential measurements were also performed to determine surface charges of the SBA, H40-MSN, aminated H40-MSN, and PEG-H40-MSNs. The zeta potential of SBA-15 was about −29 mV, and it slightly increased and changed to −22 mV by grafting hyperbranched Boltorn H40. The zeta potential of aminated H40-MSN was about +22 mV, highly positive as expected, which referred to great amount of tertiary amine groups and successful grafting DEAPA on the surface of nanoparticles [19]. After grafting PEG, the zeta potential of PEG-H40-MSNs slightly decreased to +16 mV which represented the success of the reaction [20]. These results indicated that hyperbranched-DEAPA-PEGs polymer shells were formed and provided appropriate charge density and excellent stability in aqueous environment.

PEG-H40-MSNs exhibited great drug loading capacity and Encapsulation efficiency. The reasons for showing these promising features were that at this pH value, the polymeric shell around the nanocarriers was swelled and DOX and the shell were both neutral. Hence, the repulsion force between DOX and PEG-H40-MSNs was decreased, resulted in loading almost all DOX molecules into the shell and the channels of MSN [21]. In addition, the hydrophobic form of DOX made the easy penetration of DOX into the hydrophobic hyperbranched polymeric shell and the channels of MSN possible because of the hydrophobicity interaction between them [22, 23].

In vitro release behavior of DOX-loaded PEG-H40-MSNs was evaluated at 37 °C under pH values of 7.4, 6.8, and 5.5. It can be observed that the rates of DOX release from the nanocarrier in acidic pHs were more than 7.4 in the first 48 h because at lower pH value, the tertiary amine groups of DEAPA on the hyperbranched polyester absorbed hydronium ion and the positive charge was formed between the polymer chains. Hence, electrostatic repulsion between positive charges caused swelling of the polymeric shell and led to the manifold release rate of DOX [24].

Nanoparticles can have devastating effects on the immune system, hematological factors and induce inflammatory responses [25].

ALT and AST, two important liver health indicators of two groups of treated mice (5 h and 10 days after injection), which were very close and had a good match with the control group. Also, kidney health functions had negligible diversity in contrast with the control mice. Obtained results revealed that synthesized PEG-H40-MSNs had no toxicity and had the slightest effects on the liver and kidney of treated mice at a high disposal value of 10 $mg.kg^{-1}$ until 10 days after injection.

A hybrid nanocarrier based on rod-shaped mesoporous silica and pH-responsive polymeric shell were synthesized well. BET analysis revealed that rod MSN possesses a type IV standard isotherm and TEM represented that hyperbranched H40 was grafted on the surface of SBA-15. DOX was released according to the ambient pH inside the cell. PEG-H40-MSNs showed no effect on the liver and kidney of treated mice. The in vitro cytotoxicity of the DOX-PEG-H40-MSNs generally enhanced by increasing the concentration of DOX. The synthesized hybrid nanoparticles displayed essential features that are required for drug delivery, such as lower toxicity, acceptable biocompatibility, and the ability to control DOX release in different pHs.

Conclusion

In this paper, a new approach for the functionalization of SBA-15 MSNs was developed. First, Boltorn H40 was grafted on the SBA-15 surface and, then, in order to attain pH-responsive and biocompatible particles for DOX delivery, hyperbranched polyester grafted SBA-15 was modified by tertiary amine and PEG 1000 respectively. PEG-H40-MSNs showed acceptable loading capacity (36.5%) and entrapment efficiency (57.4%). The cumulative release of DOX was only 9.7% and 20% at pH 7.4 and pH 6.8, respectively, after 48 h, while significantly increased to 49% at pH 5.5. These observations revealed that the DOX release from PEG-H40-MSNs had a pH-dependent behavior. The in vitro and in vivo results revealed that PEG-H40-MSNs possess minimum cytotoxicity, very low cytotoxicity in mice kidney and liver, and excellent blood biocompatibility. The cell viability of DOX-PEG-H40-MSNs on the MCF7 cell line was evaluated, showing the cell cytotoxicity of both pure DOX and DOX-PEG-H40-MSNs generally enhanced by increasing concentration of DOX.

Acknowledgments This work was financially supported by the Nanotechnology Research Center, Faculty of Pharmacy, Tehran University of Medical Sciences, Tehran, Iran.

Compliance with ethical standards

Conflict of interest The authors declare that they have no conflict of interest.

References

1. Pendekal MS, Tegginamat PK. Development and characterization of chitosan-polycarbophil interpolyelectrolyte complex-based 5-fluorouracil formulations for buccal, vaginal and rectal application. Daru. 2012;20(1):67. https://doi.org/10.1186/2008-2231-20-67.
2. Bafkary R, Khoee S. Carbon nanotube-based stimuli-responsive nanocarriers for drug delivery. RSC Adv. 2016;6(86):82553–65.
3. Khoee S, Saadatinia A, Bafkary R. Ultrasound-assisted synthesis of pH-responsive nanovector based on PEG/chitosan coated magnetite nanoparticles for 5-FU delivery. Ultrason Sonochem. 2017;39:144–52. https://doi.org/10.1016/j.ultsonch.2017.04.025.
4. Ziarani GM, Faramarzi S, Asadi S, Badiei A, Bazl R, Amanlou M. Three-component synthesis of pyrano[2,3-d]-pyrimidine dione derivatives facilitated by sulfonic acid nanoporous silica (SBA-Pr-SO3H) and their docking and urease inhibitory activity. Daru. 2013;21(1):3. https://doi.org/10.1186/2008-2231-21-3.
5. Li Y, Guo W, Su X, Ou-Yang L, Dang M, Tao J, et al. Small size mesoporous organosilica nanorods with different aspect ratios: synthesis and cellular uptake. J Colloid Interface Sci. 2018;512:134–40. https://doi.org/10.1016/j.jcis.2017.10.006.
6. Giglio V, Varela-Aramburu S, Travaglini L, Fiorini F, Seeberger PH, Maggini L, et al. Reshaping silica particles: Mesoporous nanodiscs for bimodal delivery and improved cellular uptake. Chem Eng J. 2018;340:148–54.
7. Shao D, Lu MM, Zhao YW, Zhang F, Tan YF, Zheng X, et al. The shape effect of magnetic mesoporous silica nanoparticles on endocytosis, biocompatibility and biodistribution. Acta Biomater. 2017;49:531–40. https://doi.org/10.1016/j.actbio.2016.11.007.
8. Hao N, Li L, Tang F. Roles of particle size, shape and surface chemistry of mesoporous silica nanomaterials on biological systems. Int Mater Rev. 2017;62(2):57–77.
9. Xu C, Niu Y, Popat A, Jambhrunkar S, Karmakar S, Yu C. Rod-like mesoporous silica nanoparticles with rough surfaces for enhanced cellular delivery. J Mater Chem B. 2014;2(3):253–6.
10. Yu T, Malugin A, Ghandehari H. Impact of silica nanoparticle design on cellular toxicity and hemolytic activity. ACS Nano. 2011;5(7):5717–28. https://doi.org/10.1021/nn2013904.
11. Khoee S, Bafkary R, Fayyazi F. DOX delivery based on chitosan-capped graphene oxide-mesoporous silica nanohybride as pH-responsive nanocarriers. J Sol-Gel Sci Technol. 2017;81(2):493–504.
12. Chen C, Zheng H, Xu J, Shi X, Li F, Wang X. Sustained-release study on Exenatide loaded into mesoporous silica nanoparticles: in vitro characterization and in vivo evaluation. Daru. 2017;25(1):20. https://doi.org/10.1186/s40199-017-0186-9.
13. Reul R, Nguyen J, Kissel T. Amine-modified hyperbranched polyesters as non-toxic, biodegradable gene delivery systems. Biomaterials. 2009;30(29):5815–24.
14. Akhtar MF, Ranjha NM, Hanif M. Effect of ethylene glycol dimethacrylate on swelling and on metformin hydrochloride release behavior of chemically crosslinked pH-sensitive acrylic acid-polyvinyl alcohol hydrogel. Daru. 2015;23:41. https://doi.org/10.1186/s40199-015-0123-8.
15. Wang J, Ayano E, Maitani Y, Kanazawa H. Enhanced cellular uptake and gene silencing activity of siRNA using temperature-responsive polymer-modified liposome. Int J Pharm. 2017;523(1):217–28.
16. Karimi M, Badiei A, Ziarani GM. A single hybrid optical sensor based on nanoporous silica type SBA-15 for detection of Pb 2+ and Iâ¯ in aqueous media. RSC Adv. 2015;5(46):36530–9.
17. Zhu Y, Tao C. DNA-capped Fe 3 O 4/SiO 2 magnetic mesoporous silica nanoparticles for potential controlled drug release and hyperthermia. RSC Adv. 2015;5(29):22365–72.
18. Wei J, Zou L, Li Y, Zhang X. Synthesis of core–shell-structured mesoporous silica nanospheres with dual-pores for biphasic catalysis. New J Chem. 2019;43(15):5833–8. https://doi.org/10.1039/c9nj00310j.
19. Benfer M, Kissel T. Cellular uptake mechanism and knockdown activity of siRNA-loaded biodegradable DEAPA-PVA-g-PLGA nanoparticles. Eur J Pharm Biopharm. 2012;80(2):247–56. https://doi.org/10.1016/j.ejpb.2011.10.021.
20. Yang J, Zhang RN, Liu DJ, Zhou X, Shoji T, Tsuboi Y, et al. Laser trapping/confocal Raman spectroscopic characterization of PLGA-PEG nanoparticles. Soft Matter. 2018;14(40):8090–4. https://doi.org/10.1039/c8sm01364k.

21. Yang H, Guo J, Tong R, Yang C, Chen JK. pH-Sensitive Micelles Based on Star Copolymer Ad-(PCL-b-PDEAEMA-b-PPEGMA)(4) for Controlled Drug Delivery. Polymers (Basel). 2018;10(4). doi:https://doi.org/10.3390/polym10040443.
22. Li X, Garamus VM, Li N, Gong Y, Zhe Z, Tian Z, et al. Preparation and characterization of a pH-responsive mesoporous silica nanoparticle dual-modified with biopolymers. Colloids Surf A Physicochem Eng Asp. 2018;548:61–9. https://doi.org/10.1016/j.colsurfa.2018.03.047.
23. Zhu J, Niu Y, Li Y, Gong Y, Shi H, Huo Q, et al. Stimuli-responsive delivery vehicles based on mesoporous silica nanoparticles: recent advances and challenges. J Mater Chem B. 2017;5(7):1339–52. https://doi.org/10.1039/c6tb03066a.
24. Chen Q, Zheng J, Yuan X, Wang J, Zhang L. Folic acid grafted and tertiary amino based pH-responsive pentablock polymeric micelles for targeting anticancer drug delivery. Mater Sci Eng C Mater Biol Appl. 2018;82:1–9. https://doi.org/10.1016/j.msec.2017.08.026.
25. Ali A, Suhail M, Mathew S, Shah MA, Harakeh SM, Ahmad S, et al. Nanomaterial induced immune responses and cytotoxicity. J Nanosci Nanotechnol. 2016;16(1):40–57. https://doi.org/10.1166/jnn.2016.10885.